J. Wang, S. Huang, W. Zuo, D. Vrabie 2021. "Occupant Preference-Aware Load Scheduling for Resilient Communities." *Energy and Buildings*, 252, pp. 111399. https://doi.org/10.1016/j.enbuild.2021.111399

Occupant Preference-Aware Load Scheduling for Resilient Communities

Jing Wang[a], Sen Huang[b], Wangda Zuo[a,c,*], Draguna Vrabie[b]

[a] University of Colorado Boulder, Department of Civil, Environmental and Architectural Engineering, Boulder, CO 80309, United States

[b] Pacific Northwest National Laboratory, 902 Battelle Blvd, Richland, WA 99354, United States

[c] National Renewable Energy Laboratory, 15013 Denver West Parkway, Golden, CO 80401, United States

Abstract

The load scheduling of resilient communities in the islanded mode is subject to many uncertainties such as weather forecast errors and occupant behavior stochasticity. To date, it remains unclear how occupant preferences affect the effectiveness of the load scheduling of resilient communities. This paper proposes an occupant preference-aware load scheduler for resilient communities operating in the islanded mode. The load scheduling framework is formulated as a model predictive control problem. Based on this framework, a deterministic load scheduler is adopted as the baseline. Then, a chance-constrained scheduler is proposed to address the occupant-induced uncertainty in room temperature setpoints. Key resilience indicators are selected to quantify the impacts of the uncertainties on community load scheduling. Finally, the proposed preference-aware scheduler is compared with the deterministic scheduler on a virtual testbed based on a real-world net-zero energy community in Florida, USA. Results show that the proposed scheduler performs better in terms of serving the occupants' thermal preference and reducing the required

* Corresponding author.
Email address: wangda.zuo@colorado.edu.

battery size, given the presence of the assumed stochastic occupant behavior. This work indicates that it is necessary to consider the stochasticity of occupant behavior when designing optimal load schedulers for resilient communities.

Keywords: Microgrid; Optimal load scheduling; Uncertainty; Occupant behavior; Resilient community; Model predictive control.

Nomenclature

Parameters		E_{bat}^{t}	battery energy
a	intercept coefficient for the logistic regression model	P_{ch}^{t}	battery charging power
b	slope coefficient for the logistic regression model	$P_{crit,j}^{t}$	scheduled critical loads
$\overline{E}_{bat}$	upper limit of battery energy	P_{curt}^{t}	curtailed PV power
e	mathematical constant	P_{dis}^{t}	battery discharging power
H	MPC prediction horizon	P_{hvac}^{t}	HVAC system (heat pump) total power
N	simulation horizon	P_{load}^{t}	total scheduled loads
N_{crit}	number of critical loads in each building	$P_{modu,j}^{t}$	scheduled modulatable loads
N_{modu}	number of modulatable loads in each building	$P_{shed,j}^{t}$	scheduled sheddable loads
N_{shed}	number of sheddable loads in each building	$P_{shif,j}^{t}$	scheduled shiftable loads
N_{shif}	number of shiftable loads in each building	P_{pv}^{t}	PV power
$n_{shif,j}$	average cycle time of each shiftable load	r_{hvac}^{t}	speed ratio of the heat pump
$\overline{P}_{bat}$	upper limit of battery power	T_{room}	indoor air temperature
$\hat{P}_{crit,j}^{t}$	critical load data	$t_{shif,j,s}$	starting operation time of shiftable loads
$P_{hvac,nom}$	HVAC system (heat pump) nominal power	Q_{gain}^{t}	internal heat gain
$\overline{P}_{load}^{t}$	predicted loads upper bound	**Binary Variables**	
$\hat{P}_{modu,j}^{t}$	modulatable load data	$u_{shed,j}^{t}$	binary decision variable for sheddable load on/off status
$\hat{P}_{shed,j}^{t}$	sheddable load data	$v_{shif,j}^{t}$	binary variable for shiftable load starting time

$P_{shif,j,avg}$	average nominal power of each shiftable load	**Abbreviations**	
p	probability of setpoint-changing actions	BAL	building agent layer
$\boldsymbol{S}_{shif,j}$	scheduling matrix for each shiftable load	CDF	cumulative distribution function
T_{amb}^{t}	ambient outdoor temperature	COL	community operator layer
$\underline{T}_{room}$	lower room temperature bound	DER	distributed energy resource
$\overline{T}_{room}$	upper room temperature bound	DR	demand response
Q_{sol}^{t}	solar irradiance	HVAC	heating, ventilation, and air-conditioning
γ	penalty coefficients	KRI	key resilience indicator
Δt	timestep	MPC	model predictive control
ϵ, ϵ_T	maximum constraint violation probability	RC	resistance-capacitance
η_{ch}	battery charging efficiency	RMSE	Root Mean Square Error
η_{dis}	battery discharging efficiency	SOC	state of charge
μ_T^t	mean of room temperature error distribution	PDF	probability density function
σ_T^t	standard deviation of room temperature error distribution	PID	proportional integral derivative
Continuous Variables		PV	photovoltaics

1 Introduction

Due to the increasing frequency of extreme weather events such as the 2021 Texas Power Crisis [1], there is an emerging need for community resilience studies. Resilient communities refer to those that can sustain disruptions and adapt to them quickly by continuing to operate without sacrificing the occupants' essential needs [2, 3]. Enabling technologies for resilient communities often involve distributed energy resources (DERs) such as photovoltaics (PV) and electrical energy storage (EES) systems. When disconnected from the main grid, the adoption of advanced control techniques can help enhance community resilience.

As an advanced control technique, optimal load scheduling determines the operation schedules of controllable devices in the community to achieve optimization objectives. For a resilient community, typical controllable assets include the EES, PV, and thermostatically controllable

devices in buildings such as the heating, ventilation, and air-conditioning (HVAC) system. Building plug loads that are sheddable, shiftable, or modulatable can also be considered flexible loads in islanded circumstances [4]. The objectives of the load scheduling for resilient communities often involve maximizing the self-consumption rate of locally generated PV energy, minimizing PV curtailment, and minimizing the unserved ratio to critical loads.

It is important to account for uncertainties when designing a load scheduler for resilient communities. Moreover, due to the limited amount of available PV generation during off-grid scenarios, the uncertainties need to be more carefully dealt with to ensure a satisfying control performance. Sources of uncertainties for a community load scheduling problem mainly lie in two aspects: power generation and consumption. For renewable energy generation, weather forecast errors play a prominent role in the cause of uncertainty. Whereas, for energy consumption, occupant behavior stochasticity is a major source of uncertainty.

Much of existing load scheduling research has considered the uncertainty of weather forecasts [5–13]. Kou [5] proposed a comprehensive scheduling framework for residential building demand response (DR) considering both day-ahead and real-time electricity markets. The results demonstrated the effectiveness of the proposed approach for large-scale residential DR applications under weather and consumer uncertainties. Garifi [13] adopted stochastic optimization in a model predictive control (MPC)-based home energy management system. The indoor thermal comfort is ensured at a high probability with uncertainty in the outdoor temperature and solar irradiance forecasts. Faraji [6] proposed a hybrid learning-based method using an artificial neural network to precisely predict the weather data, which eliminated the impact of weather forecast uncertainties on the scheduling of microgrids. Similarly, in the authors' previous publication [7], normally distributed outdoor temperature and solar irradiance forecast errors were introduced into the community control framework, which accounted for the uncertainties in the weather forecasts.

However, the uncertainties from the power consumption perspective, especially the occupant behavior uncertainty, is rarely accounted for in load scheduling research [14–18]. Some efforts to integrate occupant behavior modeling can be found in studies of building optimal control [19–22]. Aftab [19] used video-processing and machine-learning techniques to enable real-time building occupancy recognition and prediction. This further facilitated the HVAC system operation control

to achieve building energy savings. Lim [20] solved a joint occupancy scheduling and occupancy-based HVAC control problem for the optimal room-booking (i.e., meeting scheduling) in commercial and educational buildings. Both the occupancy status of each meeting room and the HVAC control variables were decision variables. Mixed-integer linear programming was adopted to optimally solve the optimization problem.

Notably, all of the preceding control work considered the stochasticity of building occupancy schedules, but the integration of other types of occupant behavior into building optimal control is not well studied in existing literature. Some researchers integrate the occupant thermal sensation feedback into the MPC for buildings [23, 24]. For instance, Chen [23] integrated a dynamic thermal sensation model into the MPC to help achieve energy savings using the HVAC control. For the occupant sensation model, the predictive performance of certainty-equivalence MPC and chance-constrained MPC were compared.

To summarize, the literature review shows that current research mainly focuses on the load scheduling of single buildings under grid-connected scenarios. There is a lack of research on the optimal load scheduling of resilient communities informed by occupant behavior uncertainties in the islanded mode. Given this gap, this paper proposes an occupant preference-aware load scheduling framework for resilient communities in the islanded mode. The occupants' thermal preference for indoor air temperature will be reflected in the integration of thermostat adjustment probabilistic models. The optimal load scheduling is formulated as an MPC problem, so the stochastic thermostat-changing behavior will be regarded as the uncertainty in the MPC problem. Different methods, such as the offset-free method and robust method, can be used to handle the uncertainties in MPC problems [25]. The chance-constraint method, also known as the stochastic MPC, was selected to deal with the uncertainty in occupant preference in our study. It allows the violation of certain constraints at a predetermined probability. It thus enables a systematic trade-off between the control performance and the constraint violations [26]. The advantage of addressing occupant preference uncertainty by using the chance-constraint method lies in the *a priori* handling of the uncertainty, which does not require the extra error-prediction models needed by other methods (i.e., offset free method), and thus simplifies the control problem [27]. Therefore, less computational effort is required after the control design phase. Though it requires the

controller to know the estimated uncertainty distribution beforehand, the development of occupant behavior probabilistic modeling will make knowing this less challenging.

In this work, we consider the load scheduling of a resilient community in islanded mode during power outages. The goal is to study the impact of occupants' thermal preference on the operation of an islanded community. The load scheduling problem of the community will be solved using an optimization-based hierarchical control framework. Occupant thermal preference will be integrated through thermostat changing behavioral models to inform the development of the load scheduler. The major contributions of this work include (1) a proposed new preference-aware load scheduler for resilient communities, which assures better control performance related to satisfying occupants' thermal preferences and reducing the battery size; (2) the quantification of the impact of occupant thermostat-changing behavior on resilient community optimal scheduling using selected key resilience indicators (KRIs); and (3) the testing of the proposed scheduler on a high-fidelity virtual testbed for resilient communities.

The remainder of this paper is organized as follows: Section 2 details the research methodology. Section 3 describes the controllable device models used in this work involving the building HVAC models, load models, and battery models. Section 4 then discusses the deterministic versus stochastic scheduler formulations and proposes a chance-constrained controller for preference-aware load scheduling of resilient communities. Section 5 applies the theoretical work to a case study community and quantifies the impact of occupant preference uncertainty. Simulation results and discussions are presented in this section. Finally, Section 6 concludes the paper by identifying future work.

2 Methodology

In this section, we first introduce a hierarchical optimal control structure for resilient community load scheduling. Based on the structure, a deterministic scheduler will be implemented as the baseline. Further, we propose a research workflow to implement a stochastic preference-aware scheduler for addressing uncertainties in occupant thermostat-changing behavior. KRIs are proposed at the end of this section.

2.1 Hierarchical Optimal Control for Resilient Communities

In this study, we assume that the only energy resource accessible to the islanded community is on-site PV generation and the batteries for an extended period of more than 24 hours. In this problem setting, in order to make full use of the limited amount of PV generation and satisfy the occupants' essential needs, the building loads need to be shifted or modulated. The battery works as a temporal arbitrage for meeting the demand at night. In addition, the occupant thermal preference will affect the energy consumption of the HVAC system through the stochastic thermostat-changing behavior. To optimally control such a community, considering the above factors, we adopted a hierarchical control structure.

As illustrated in Figure 1, two layers of control are formulated: a community operator layer (COL) and a building agent layer (BAL). The COL optimally allocates the limited amount of the on-site PV generation based on the load flexibility provided by each building. The calculated allowable load for each building is then passed down to the BAL, where each building optimally schedules its controllable devices (i.e., HVAC, battery, and controllable loads) to achieve its local optimization goals. Both layers are formulated as MPC-based optimization problems.

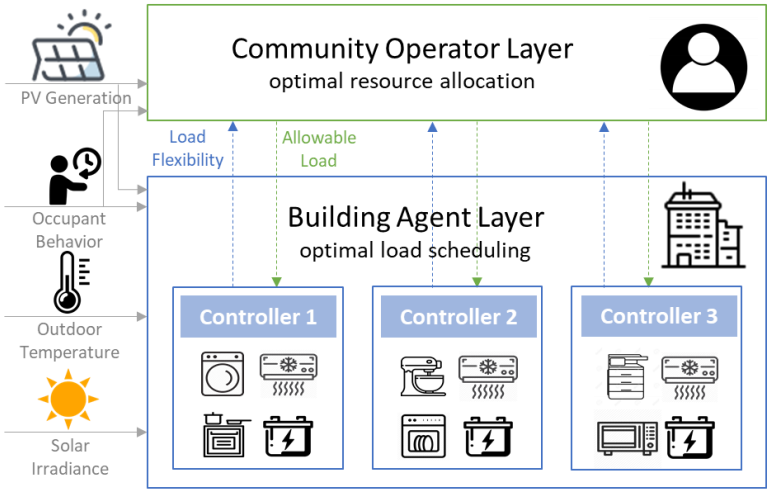

Figure 1 The hierarchical optimal control structure for community operation.

The input of the hierarchical control involves the predicted PV generation data, outdoor air dry-bulb temperature, and solar irradiance. The PV generation data are used by the COL to determine the optimal allocation among buildings. The temperature and irradiance data are used by the HVAC models for updating the indoor room temperature predictions. The occupant behavior

affects the two layers differently. The COL uses building occupancy schedules to decide the weights of different buildings during the PV allocation (details can be found in [7]). The BAL considers occupant thermal preference to be the uncertainty in the indoor room temperature prediction.

2.2 Proposed Workflow

Figure 2 depicts the workflow of this paper. A deterministic optimal load scheduler without the occupant thermal preference uncertainty is implemented in the hierarchical control structure. Further, to account for the uncertainties, we propose a chance-constrained controller. It is developed based on the deterministic controller and involves an alteration of the room temperature constraints, which accounts for the uncertainties in room temperature prediction errors caused by the occupants' thermostat-changing behavior. The Monte Carlo simulation method was adopted to cover a wide range of simulation results.

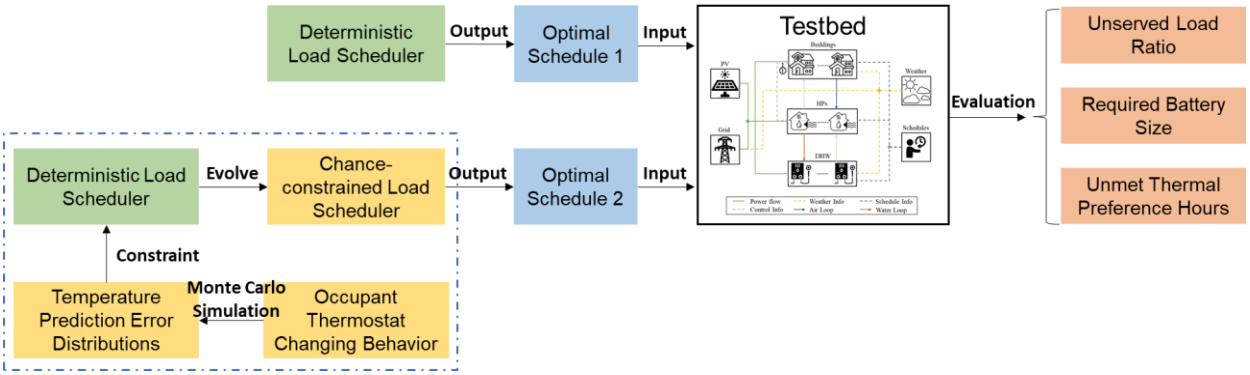

Figure 2 Diagram of the proposed workflow.

Further, to reflect various styles of occupant behavior, three types of occupant thermostat-changing models were adopted: low, medium, and high, which represent three levels of frequencies of the thermostat-changing activities. Here, we assume that when the occupant decides to change the indoor air temperature setpoint according to their preference, the predetermined optimal HVAC equipment control setting at the current timestep will be overridden. Instead, a new control setting will be calculated to achieve the occupants' setpoint at the current timestep. At the next timestep, the predetermined optimal setting will still be used if the occupant is not changing the setpoint consecutively.

Finally, the optimal schedules determined by the chance-constrained controller and the deterministic controller are tested on a high-fidelity virtual testbed [28] with respect to their individual performances. KRIs such as the unserved load ratio, the required battery size, and the unmet thermal preference hours were adopted to quantify the results.

The *unserved load ratio* in this paper is defined as the relative discrepancy between the served load P_{load}^{t} and the originally predicted load $\overline{P}_{load}^{t}$:

$$Unserved\ load\ ratio = \frac{\sum_{t=1}^{N}\left(\overline{P}_{load}^{t} - P_{load}^{t}\right)}{\sum_{t=1}^{N}\overline{P}_{load}^{t}}, \tag{1}$$

where N is the MPC simulation horizon of 48 hours. The *required battery size* is obtained by subtracting the minimum battery SOC from the maximum SOC. This gives us a sense of how much of the battery capacity has been used under different scenarios. Finally, we define the *unmet thermal preference hours* metric for the cumulative absolute difference between the actual and the preferred room temperature over the optimization horizon:

$$Unmet\ thermal\ preference\ hours = \sum_{t=1}^{N}\left|T_{room}^{t} - T_{prefer}^{t}\right|\Delta t. \tag{2}$$

It quantifies how well the controller performs to satisfy the occupants' thermal preference and has the unit of ºC·h (degree hours).

3 Models for Controllable Devices

3.1 HVAC Models

This study assumes that heating and cooling is provided by heat pumps and the heat pump energy consumption represents the HVAC system energy consumption. We adopted linear regression models for the HVAC system to predict room temperatures at each timestep. To precisely model the building thermal reactions, two types of parameters that contribute to the heat gain of the building space are considered. The first type is environmental parameters such as the outdoor air dry-bulb temperature and solar irradiance. The second type represents the internal heat gain due to the presence of the occupants and the operation of appliances. We assumed that the simulated buildings are well sealed and thus the interference from the infiltration can be omitted. Therefore, the HVAC model updates the indoor room temperature based on the room temperature at the last

timestep, the abovementioned heat gains, and the heating/cooling provided by the heat pump system at every timestep. The control variable is the heat pump speed ratio, which ranges from 0 to 1 continuously. The resulting HVAC power is equal to the speed ratio multiplied by the nominal heat pump power. Additionally, to better account for the effect of building thermal mass, for each heat gain parameter, two past terms are adopted, respectively [29]. The equations for the HVAC model are as follows:

$$T_{room}^{t+1} = \beta_1 T_{room}^{t} + \beta_2 T_{room}^{t-1} + \beta_3 T_{amb}^{t} + \beta_4 T_{amb}^{t-1} + \beta_5 r_{hvac}^{t} + \beta_6 Q_{sol}^{t} + \beta_7 Q_{sol}^{t-1} + \beta_8 Q_{gain}^{t} + \beta_9 Q_{gain}^{t-1}, \quad (3)$$

$$\text{s.t. } 0 \le r_{hvac}^{t} \le 1, \quad (4)$$

$$P_{hvac}^{t} = r_{hvac}^{t} P_{hvac,nom}, \quad (5)$$

where T_{room}^{t}, T_{amb}^{t}, Q_{sol}^{t}, and Q_{gain}^{t} represent the room temperature, ambient dry-bulb temperature, solar irradiance, and internal heat gain at timestep t, respectively. The r_{hvac}^{t} and $P_{hvac,nom}$ are the heat pump speed ratio and the nominal HVAC system power. The linear regression coefficients are represented by β. For β_5, a negative value means cooling and positive means heating.

In the model, Q_{gain}^{t} and Q_{gain}^{t-1} are related to the occupant presence and the operation of the building appliances. When the building is occupied, 70% of the total heat rate of a person (i.e., 100 W) is dissipated as sensible heat into the space and the rest 30% is latent heat [30]. The heat gain from appliances is calculated by the power of the appliance multiplied by its heat gain coefficient, which reflects how much of the consumed electric power is dissipated into the space as heat. Table A-1 in Appendix A lists the heat gain coefficients adopted from literature [31–33]. Note that the controllable loads are optimization variables of the scheduling problem, which will be iteratively calculated at each optimization timestep. Therefore, to speed up the optimization, we reduced the coupling between the thermal models and the electric demand models. This was done by calculating the weighted average heat gain coefficients for each building based on the capacity of each appliance (Table A-1).

3.2 Load and Battery Models

The building load models in this work are categorized into four types according to their power flexibility characteristics: sheddable, modulatable, shiftable, and critical (Figure 3). We did the categorization from the perspective of the building owners during power outages. The sheddable loads are those that can be disconnected without affecting the occupants' essential needs. For instance, the microwave in a bakery is categorized as sheddable during an outage. The modulatable loads are the systems that have varying power shapes such as an HVAC system with a variable frequency drive. The shiftable loads are the appliances that have flexible operation schedules such as washers and dryers. Lastly, the critical loads refer to appliances and systems related to the occupants' essential needs. In this work, we consider only loads used for lighting and food preservation as critical loads, which aligns with the two bottom levels of Maslow's Hierarchy of Needs (i.e., physiological and safety needs) [34]. The critical loads account for about 20% to 90% of the total building loads depending on building type and time of day.

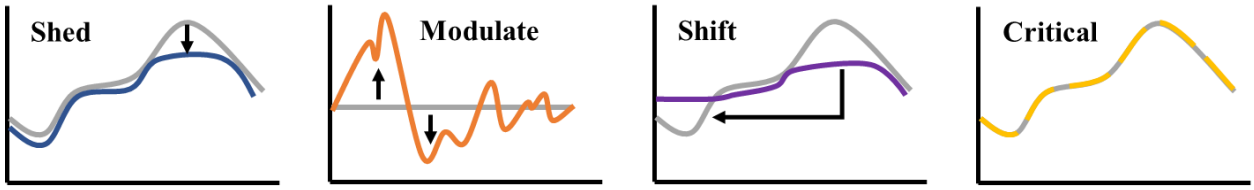

Figure 3 Power flexibility characteristics of the four load types [35].

The mathematical formulation of the sheddable load is shown in Equation (6):

$$P^t_{shed,j} = u^t_{shed,j}\hat{P}^t_{shed,j}, \qquad j \in \{1, \dots, N_{shed}\}, \tag{6}$$

where $u^t_{shed,j}$ is a binary optimization variable, $\hat{P}^t_{shed,j}$ is the original sheddable load time series data, and N_{shed} is the number of sheddable loads in the building. The actual sheddable load after optimization $P^t_{shed,j}$ is determined by the ON/OFF status represented by the binary variable. The modulatable load $P^t_{modu,j}$ is formulated as a continuous optimization variable, which ranges between zero and its original power demand $\hat{P}^t_{modu,j}$. Equation (7) sets the lower and upper bound of the modulatable load.

$$0 \le P^t_{modu,j} \le \hat{P}^t_{modu,j}, \qquad j \in \{1, \dots, N_{modu}\}. \tag{7}$$

The shiftable loads are scheduled through scheduling matrices [36]. First, using the power data [37], we extracted the average cycle time $n_{shif,j}$ and the average power demand $P_{shif,j,avg}$ of each shiftable load. The starting operation timestep $t_{shif,j,s}$ of each shiftable load is optimized over the MPC horizon. At the scheduled starting timestep, the binary variable $v^t_{shed,j}$ equals 1 and is 0 otherwise:

$$v^t_{shif,j} = \begin{cases} 1, t = t_{shif,j,s}, \\ 0, t \neq t_{shif,j,s}, \end{cases} \quad \forall t \in \{1, \dots, H - n_{shif,j} + 1\}, \qquad j \in \{1, \dots, N_{shif}\}. \tag{8}$$

H is the MPC prediction horizon. Once the starting time of a shiftable load is selected, the power demand of the load is then fixed at its average power until it finishes its cycle. The appliance must finish its cycle before the horizon ends ($t \in \{1, \dots, H - n_{shif,j} + 1\}$). Here, we assume that each shiftable load operates once and only once during each horizon, which is enforced by:

$$\sum_{t=1}^{H-n_{shif,j}+1} v^t_{shif,j} = 1. \tag{9}$$

Next, a scheduling matrix $\boldsymbol{S}_{shif,j}$ of shape $H \times (H - n_{shif,j} + 1)$ is generated for each shiftable load. The actual power shape of the load, denoted $P^t_{shif,j}$, is thus calculated by:

$$P^t_{shif,j} = \boldsymbol{S}_{shif,j} \times \begin{bmatrix} v^1_{shif,j} \\ \vdots \\ v^{H-n_{shif,j}+1}_{shif,j} \end{bmatrix} \times P_{shif,j,avg}. \tag{10}$$

Finally, the actual critical load $P^t_{crit,j}$ must be exactly equal to the critical power demand $\hat{P}^t_{crit,j}$, as enforced by:

$$P^t_{crit,j} = \hat{P}^t_{crit,j}, \qquad j \in \{1, \dots, N_{crit}\}. \tag{11}$$

Summing up the four types of loads in each building, we obtain the optimization variable P^t_{load} as follows:

$$P^t_{load} = \sum_{j=1}^{N_{shed}} P^t_{shed,j} + \sum_{j=1}^{N_{modu}} P^t_{modu,j} + \sum_{j=1}^{N_{shif}} P^t_{shif,j} + \sum_{j=1}^{N_{crit}} P^t_{crit,j}. \tag{12}$$

The linear battery model adopted in this work is represented by Equation (13). The battery state of charge (SOC) E_{bat}^{t+1} is predicted based on the SOC of the previous timestep E_{bat}^{t}, the battery charging P_{ch}^{t} or discharging power P_{dis}^{t} at each step, and the battery charging/discharging efficiencies η_{ch} and η_{dis}. The inequality constraints in Equations (14) and (15) enforce the acceptable limits for the battery charging/discharging power and SOC, where $\overline{P}_{bat}$ and $\overline{E}_{bat}$ are the maximum values for battery power and capacity:

$$E_{bat}^{t+1} = E_{bat}^{t} + \eta_{ch} P_{ch}^{t} \Delta t - \frac{1}{\eta_{dis}} P_{dis}^{t} \Delta t, \tag{13}$$

$$\text{s.t. } 0 \le P_{ch}^{t}, P_{dis}^{t} \le \overline{P}_{bat}, \tag{14}$$

$$0 \le E_{bat}^{t+1} \le \overline{E}_{bat}. \tag{15}$$

4 Optimal Load Scheduling

This section first presents the mathematical formulation of the deterministic load scheduler. After that, we will introduce the formulation of the occupant preference-aware stochastic scheduler containing three parts: the thermostat-changing model, the uncertainty introduction mechanism, and the method to address the uncertainty.

4.1 Deterministic Scheduler

As introduced in Section 2.1, the deterministic scheduler adopts a two-layer structure with COL and BAL. The objective of the COL is to minimize the community-level PV curtailment to facilitate better use of the limited PV power during the outage. The main constraints are the load flexibility of each building, building occupancy, and building priority, etc. No detailed building assets are simulated at the community layer. This ensures that the COL is computationally tractable, especially when the problem scales up and the number of controllable building assets scales up. The detailed mathematical formulation of the COL can be found in reference [7].

The objective of the BAL is to minimize the unserved load ratio of each building within the allowable load range allocated by the COL. This is achieved through MPC-based optimal scheduling of the building-owned HVAC system, controllable loads, and battery. The optimization

is a mixed-integer linear programming problem, because the sheddable and shiftable load models contain binary variables. Next, the mathematical formulation of the optimization problem is presented. Note that the formulation applies for every individual building in the community.

The cost function to minimize the unserved load ratio is formulated as:

$$f_{cost}(t, \{x^t\}_{t=1}^{H}) = \sum_{t=1}^{H} \left(\overline{P}_{load}^{t} - P_{load}^{t}\right) + \sum_{t=1}^{H} \gamma P_{ch}^{t} + \sum_{t=1}^{H} \gamma' P_{curt}^{t}, \tag{16}$$

$$\min_{\{x^t\}_{t=1}^{H}} f_{cost}(t, \{x^t\}_{t=1}^{H}), \tag{17}$$

where $\overline{P}_{load}^{t}$ is the predicted load upper bound from data. The difference between this upper bound and the actual operated loads P_{load}^{t} is minimized to achieve a maximum served load to the building. To avoid simultaneous battery charging and discharging as well as PV curtailment, the objective function also includes small penalizations of charging γP_{ch}^{t} and curtailment $\gamma' P_{curt}^{t}$ [38], where γ and γ' are the penalization coefficients. The power balance of each building that must be satisfied at each timestep is given by:

$$P_{pv}^{t} - P_{curt}^{t} = P_{ch}^{t} - P_{dis}^{t} + P_{load}^{t} + P_{hvac}^{t}, \tag{18}$$

where PV curtailment P_{curt}^{t} is limited by how much PV generation P_{pv}^{t} is available:

$$0 \leq P_{curt}^{t} \leq P_{pv}^{t}. \tag{19}$$

The left-hand side of Equation (18) represents power generation, whereas the right-hand side represents consumption. The P_{ch}^{t} and P_{dis}^{t} stand for the battery charging and discharging power as in Equation (13). The P_{load}^{t} and P_{hvac}^{t} are the total building loads and the HVAC power calculated in Equations (12) and (5), respectively. To assure thermal comfort of the indoor environment, a temperature constraint is given by:

$$\underline{T}_{room} \leq T_{room}^{t} \leq \overline{T}_{room}, \tag{20}$$

where $\underline{T}_{room}$ and $\overline{T}_{room}$ are the lower and upper room temperature bounds implemented as hard constraints. The optimization variables in each building agent are collected in vector x^t:

$$x^t = \begin{bmatrix} \{P^t_{curt}\}^H_{t=1}, \{P^t_{ch}\}^H_{t=1}, \{P^t_{dis}\}^H_{t=1}, \{r^t_{hvac}\}^H_{t=1}, \{u^t_{shed,j}\}^H_{t=1}, \\ \{P^t_{modu,j}\}^H_{t=1}, \{v^t_{shif,j}\}^{H-n_{shif,j}+1}_{t=1}, \{T^t_{room}\}^H_{t=1}, \{E^t_{bat}\}^H_{t=1} \end{bmatrix}. \quad (21)$$

4.2 Stochastic Preference-aware Scheduler

To address the uncertainties of occupant thermal preference in the scheduling problem of resilient communities, this section introduces the stochastic preference-aware scheduler. First, we discuss the modeling of the occupant behavior uncertainties as a probability function. Then we show the mechanism by which this uncertainty might affect the optimal control of the HVAC system. After that, we propose using the chance-constraint method to address the uncertainty.

4.2.1 Stochastic Thermostat-Changing Model

The stochastic occupant thermostat-changing model adopted in this paper was proposed by Gunay et al. [39]. Through continuous observation of the occupants' thermostat keypress actions in private office spaces, the relationship between the thermostat-changing behavior and the concurrent occupancy, temperature, and relative humidity was analyzed. It was noted that the frequency of thermostat interactions (i.e., increasing or decreasing) can be approximated as a univariate logistic regression model with the indoor temperature as the independent predictor variable. Though the original data set was obtained from two office buildings, Gunay et al. generalized the study to understand occupants' thermostat user behavior and temperature preferences. Given the universality of their work, we have adapted their models based on our use cases. Note that occupants might have varied (e.g., higher) tolerance of indoor temperature during an emergency situation. The exact thresholds need further experimental study and validation, which is out of the scope of this work.

The thermostat-changing behavior models determine whether the occupants will change the setpoint temperature based on the concurrent indoor air temperature. The probability of increasing and decreasing the temperature setpoint is predicted with a logistic regression model:

$$p = \frac{1}{1 + e^{-(a+bT_{room})}}, \quad (22)$$

where p is the probability of the changing action, T_{room} is the indoor room temperature, and a and b are coefficients. To investigate different uncertainty levels, we proposed three different active

levels by revising the coefficients of the model in Equation (22). As shown in Table 1, the low active level adopts the original coefficients in [39]. Then, we proposed the medium and high active levels to represent various occupant thermal preference styles. The standard errors and p-values of the low active level coefficients are also provided in the table. As for the medium and high levels, we do not have measurement data for the statistical analysis since we adapted the coefficients from the original reference [39].

Table 1 Coefficients in different active levels of the occupant thermostat-changing behavior model.

Active Level	**Coefficients**			
	Increasing		**Decreasing**	
	a	**b**	**a**	**b**
Low [39]	-0.179	-0.285	-17.467	0.496
Medium	7.821	-0.485	-20.667	0.696
High	15.821	-0.685	-23.867	0.896
Standard Error	1.047	0.048	0.684	0.028
p-value	0.864	0.000	0.000	0.000

Note that the adaptation of the original logistic regression models was made under the following assumptions to ensure the adapted models remained realistic. For the setpoint increasing scenario, the slope coefficient of b is varied linearly to reflect a higher frequency of the changing behavior. The intercept coefficient a is then calculated to make sure that all active levels have the same value of probability at the temperature of 40ºC. For the setpoint decreasing scenario, a similar approach is taken to make sure the same value of probability at 16ºC is shared by all active levels. At each thermostat interaction, we assume that 1ºC of setpoint change would take place. Figure 4 depicts the probabilities of the three active levels. Note that this figure contains a wider temperature range than 16ºC ~ 40ºC to show a more comprehensive performance of the behavior models.

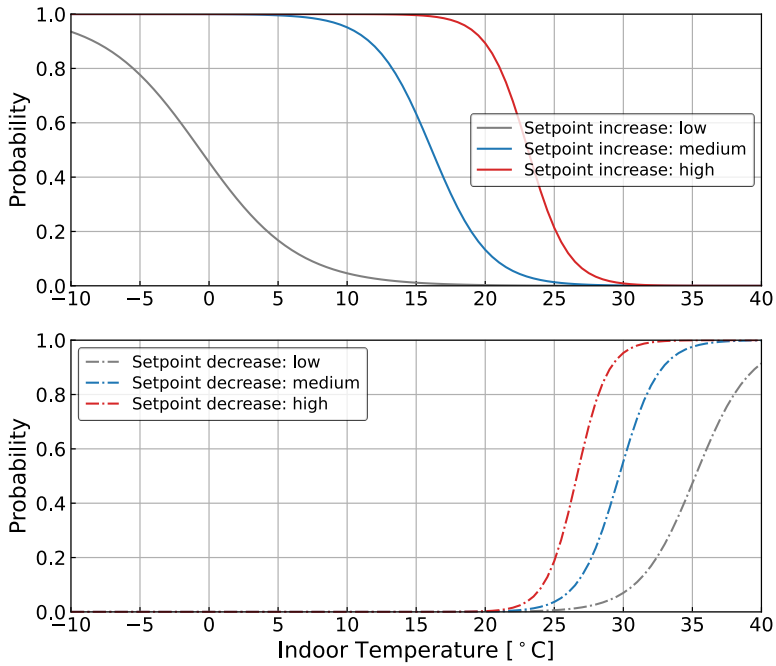

Figure 4 Probability of different thermostat-changing behavior.

Once the probability of the thermostat-changing behavior is determined using the above models, the increasing or decreasing action is determined by comparing the probabilities with a randomly generated number. At each optimization timestep, a random number between 0 and 1 is generated. If the number is larger than $1 - \Pr(increase)$, the action will be to increase. On the contrary, if it is smaller than $\Pr(decrease)$, the action will be to decrease. Because the sum of the increase and decrease probabilities is smaller than 1 in our case, this algorithm assures at most one action will be taken at each timestep.

4.2.2 Introducing Occupant Behavior Uncertainties in Scheduling

To introduce the occupant thermostat-changing uncertainties to the load scheduling problem, a stochastic simulation model representing the behavior needs to be incorporated into the optimization. Figure 5 shows the control signal flow for the typical indoor air temperature control, which affects the HVAC system operational status and its power consumption. The occupant sets the temperature setpoint according to his/her preference through the thermostat. Behind the thermostat, a proportional integral derivative (PID) controller decides the next heat pump speed to offset the difference between the measured room temperature and the setpoint. This heat pump speed signal is then fed into the heat pump system to provide cooling for the conditioned space.

Due to the presence of the dynamic environmental and behavioral disturbances, this process will need to be repeated until the measured room temperature reaches the setpoint.

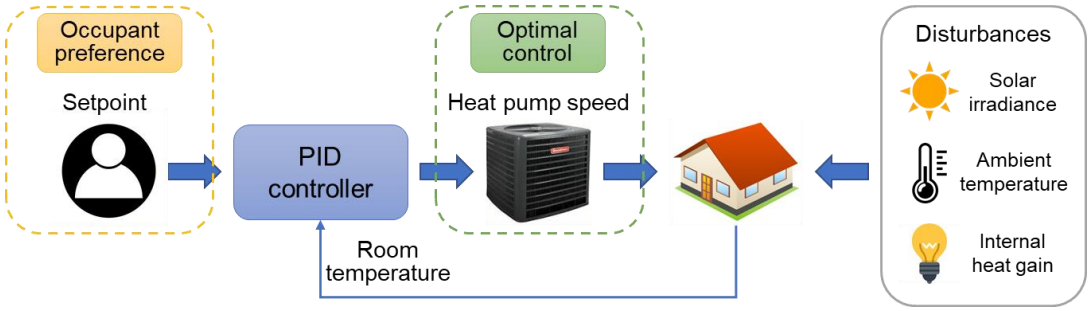

Figure 5 Diagram showing the introduction of occupant thermostat-changing behavior to the optimization.

However, in the optimal control mechanism, the optimal scheduler takes over the control of the heat pump speed from the PID controller. As a result, the occupants' preference has thus been "disabled" to allow an optimal control determined by the scheduler. To mimic the overriding of the room temperature setpoint by the occupants, the following algorithm was implemented in the MPC problem and the pseudo code is shown below. Before each round of the optimization starts (Steps 1–2), if the occupant decided to change the setpoint (Step 3), the heat pump speed for the current timestep should be calculated to reach the setpoint instead of achieving the optimization objective (Steps 4–7). Otherwise, the optimization runs normally because no overriding happens (Step 7). After each optimization timestep, the flag variables indicating the thermostat-changing actions need to be updated according to the concurrent room temperature (Step 8). It should be noted that in the optimization, no PID controller has been implemented, so we assumed that $T_{room}^{t} = T_{set}^{t}$ and the setpoint changes were directly added to the room temperature T_{room}^{t}.

Step 1. Start
Step 2. Initialization of flag variables: $increase = false, decrease = false$;
Step 3. If $increase = true$ or $decrease = true$: **Step 4** $T_{room}^{t} = T_{room}^{t-1} + 1$ or $T_{room}^{t} = T_{room}^{t-1} - 1$; **Step 5** Calculate the corresponding r_{hvac}^{t}; **Step 6** Disable r_{hvac}^{t} from the optimization variables;
Step 7. Run MPC for timestep t;

Step 8. Update flag variables (i.e., $increase$ and $decrease$) according to T_{room}^{t};
Step 9. Repeat Steps 3–8 until the end of the MPC horizon of 48 hours;
Step 10. End

4.2.3 Chance-Constraint Method

As mentioned in Section 4.2.1, the uncertainties in the occupants' thermostat-changing behavior are a probability function. In the scheduling optimization problem, the constraint directly affected by the occupants' thermostat-changing behavior is the room temperature bounds. The uncertainties related to the occupants' adjusting the thermostat could lead to the violation of the temperature bounds during the implementation of the developed control strategies. Furthermore, this could lead to other control-related performances being affected, including higher building load unserved ratio and larger required battery size. To address this, we adopted the chance-constraint method.

By definition, the chance constraint allows the violation of a certain constraint with a small probability, which thus presents a systematic trade-off between control performance and probability of constraint violations [40]. It can be expressed in general by the following equation:

$$Pr(g(x,\xi) \leq 0) \geq 1 - \epsilon, \tag{23}$$

where $g(x,\xi) \leq 0$ is the inequivalent constraint and ϵ is the maximum violation probability. Given the uncertainties in the occupants' thermostat-changing behavior, we assume that the temperature bounds can be satisfied with a probability of $(1-\epsilon_T)$. For the lower temperature bounds, the chance constraint can thus be written as:

$$Pr\left(\underline{T}_{room} \leq T_{room}^{t+1}\right) \geq 1 - \epsilon_T. \tag{24}$$

Then, we rewrite it as:

$$Pr(\chi_T^{t+1} \leq 0) \geq 1 - \epsilon_T, \tag{25}$$

where $\chi_T^{t+1} = \underline{T}_{room} - T_{room}^{t+1}$. Let the indoor temperature be rewritten in terms of the prediction error: $T_{room}^{t} = T_{room,f}^{t} + T_{room,e}^{t}$ where $T_{room,f}^{t}$ is the predicted indoor room temperature and $T_{room,e}^{t}$ is the error caused by uncertainties. Similarly, $T_{room}^{t-1} = T_{room,f}^{t-1} + T_{room,e}^{t-1}$. For both timesteps, the room temperature distribution error follows the same distribution. The hypothetical

error distributions can be in different forms and here we assume the distribution to be normal. Hence, it can be represented by:

$$T_{room,e}^{t,t-1} \sim \mathcal{N}(\mu_T^t, (\sigma_T^t)^2). \tag{26}$$

Therefore, χ_T^{t+1} is also normally distributed with the following mean μ^t and standard deviation σ^t:

$$\begin{aligned}\mu^t = \underline{T}_{room} - \beta_1(T_{room}^t + \mu_T^t) - \beta_2(T_{room}^{t-1} + \mu_T^t) - \beta_3 T_{amb}^t - \beta_4 T_{amb}^{t-1} - \beta_5 r_{hvac}^t - \beta_6 Q_{sol}^t \\ - \beta_7 Q_{sol}^{t-1} - \beta_8 Q_{gain}^t - \beta_9 Q_{gain}^{t-1},\end{aligned} \tag{27}$$

$$\sigma^t = \sqrt{(\beta_1\sigma_T^t)^2 + (\beta_2\sigma_T^t)^2}. \tag{28}$$

The chance constraint can thus be reformulated as:

$$Pr(\chi_T^{t+1} \le 0) = \Phi\left(\frac{0-\mu^t}{\sigma^t}\right) \ge 1 - \epsilon_T, \tag{29}$$

where $\Phi(\cdot)$ is the cumulative distribution function (CDF) of the standard normal distribution $\mathcal{N}(0,1)$. By taking the inverse CDF of both sides, we can get:

$$\frac{0-\mu^t}{\sigma^t} \ge \Phi^{-1}(1-\epsilon_T). \tag{30}$$

Rearrange the above equation and substitute μ^t and σ^t with Equations (27) and (28). Finally, we obtain the chance constraint for ensuring the indoor temperature will not fall below the lower bound of $\underline{T}_{room}$ with the probability of $(1-\epsilon_T)$ as follows:

$$\begin{aligned}\beta_1(T_{room}^t + \mu_T^t) + \beta_2(T_{room}^{t-1} + \mu_T^t) + \beta_3 T_{amb}^t + \beta_4 T_{amb}^{t-1} + \beta_5 r_{hvac}^t + \beta_6 Q_{sol}^t + \beta_7 Q_{sol}^{t-1} \\ + \beta_8 Q_{gain}^t + \beta_9 Q_{gain}^{t-1} - \underline{T}_{room} \ge \Phi^{-1}(1-\epsilon_T)\sqrt{(\beta_1\sigma_T^t)^2 + (\beta_2\sigma_T^t)^2}.\end{aligned} \tag{31}$$

Substituting Equation (3) into (31) and rearranging, we have:

$$T_{room}^{t+1} - \underline{T}_{room} \ge \Phi^{-1}(1-\epsilon_T)\sqrt{(\beta_1\sigma_T^t)^2 + (\beta_2\sigma_T^t)^2} - (\beta_1\mu_T^t + \beta_2\mu_T^t). \tag{32}$$

Similarly, we have Equation (33) for the upper bound,

$$Pr\left(\overline{T}_{room} \ge T_{room}^{t+1}\right) \ge 1 - \epsilon_T. \tag{33}$$

Taking a similar derivation process as that in Equations (24) to (32), we can obtain the chance constraint for the temperature upper bound:

$$\overline{T}_{room} - T_{room}^{t+1} \geq \Phi^{-1}(1-\epsilon_T)\sqrt{(\beta_1\sigma_T^t)^2 + (\beta_2\sigma_T^t)^2} + (\beta_1\mu_T^t + \beta_2\mu_T^t). \quad (34)$$

The updated inequivalent constraints indicate that the temperature bounds for the optimization should be narrower than the original temperature bounds to account for the setpoint behavioral uncertainty, which is consistent with the expectations. Note that because the uncertainty-dealing method is focused on the temperature constraints, one possible limitation is that the above method might have limited effect on the controller design for buildings that have larger thermal masses, because the building temperature is insensitive to temperature constraints. More discussion of this point follows in Section 5.3.1.

5 Case Study

5.1 Studied Community

The case study community is a net-zero energy community located in Anna Maria Island, Florida, USA, which is a cooling dominated region. The community buildings are installed with both roof-top PV panels and solar carports, which harvest about 85 MWh annually for the whole community. A centralized ground source heat pump system provides the HVAC needs of the whole community with high efficiency. Other sustainable features include well-insulated building envelopes, solar thermal water heating, and rainwater recycling. This community achieved net-zero energy in the year of 2014. In the community, there are various building types such as residential, small office, gift shop, etc. We would like to cover both residential and commercial buildings in the case study. So, we selected one residential and two small commercial buildings based on the measurement data quality. More specifically, the selected three buildings consist of a residential building (area: 93.8 m^2), an ice cream shop (area: 160.5 m^2), and a bakery (area: 410 m^2). The building layout of the community can be found in reference [28].

For the given community, a virtual testbed based on the object-oriented modeling language Modelica [41] was built and validated [42]. In the testbed, the Typical Meteorological Year 3 data for a nearby city, Tampa, was adopted for this case study. The building thermal models are resistance-capacitance (RC) network models. For the optimal control in this work, the HVAC

models were trained using one month (i.e., August) of the simulation data exported from the testbed. Table 2 lists the coefficients for the linear regression HVAC models, the Root Mean Square Error (RMSE) of the models, as well as the corresponding nominal heat pump power. The N/A in the table represents a coefficient that is too small and thus has been neglected in the model. Three effective decimal places are provided.

Table 2 Coefficients and nominal power of the HVAC models.

		Residential	**Ice Cream Shop**	**Bakery**
Coefficients	T_{room}^{t}	1.429	0.502	0.977
	T_{room}^{t-1}	-0.432	0.498	0.0213
	T_{amb}^{t}	0.0263	0.000295	0.00405
	T_{amb}^{t-1}	-0.0232	-0.000193	-0.00196
	r_{hvac}^{t}	-0.210	-0.0114	-0.178
	Q_{sol}^{t}	0.0151	0.0000345	0.0107
	Q_{sol}^{t-1}	-0.00302	0.000181	-0.00621
	Q_{gain}^{t}	0.00852	N/A	N/A
	Q_{gain}^{t-1}	N/A	N/A	0.0140
RMSE [℃]		0.160	0.0205	0.114
Nominal Power [kW]		2.140	2.830	3.770

Additionally, Table 3 lists the load categorization for the studied buildings following the principles proposed in Section 3.2. A complete list of the building load capacities and their heat gains can be found in Appendix A.

Table 3 Building loads categorized into four types.

	Residential	**Ice Cream Shop**	**Bakery**
Sheddable	Computer	Coffee maker, soda dispenser, outdoor ice storage	Microwave
Modulatable	HVAC	HVAC	Mixer, unspecific room plug loads, HVAC

	Residential	Ice Cream Shop	Bakery
Shiftable	Range, washer, dryer	None	Range, oven, dishwasher
Critical	Lights, refrigerator	Lights, cooler, display case	Lights, cooler, display case

We designed three uncertainty levels (i.e., low, medium, high) as in Table 1 to evaluate the deterministic and preference-aware schedulers in this paper. They are compared to the baseline scenario, where the deterministic scheduler is applied without occupant behavior uncertainties. The following results and discussion are all based on these scenarios. All scenarios were run in the three buildings for 48 hours with a timestep of 1 hour in the islanded mode.

5.2 Settings of Chance-Constrained Controllers for Different Buildings

The preference-aware schedulers use chance-constrained controllers, whose settings depend on individual building properties and uncertainty levels. Following the method proposed in Section 4.2.3, this section provides the details of the chance-constrained controller settings for three individual buildings in the case study, which is based on the control outcome of the deterministic schedulers under three uncertainty levels.

Considering the occupant-preference-driven actions as the source of "prediction errors" for the room temperature, we extracted the distributions of the room temperature prediction errors. The Monte Carlo simulation method [43] was adopted, where 100 repeated simulations were run using the deterministic scheduler with three uncertainty levels. We used the room temperature of the deterministic baseline scenario as the benchmark to calculate the errors caused by the occupant setpoint-changing behavior. To describe the room temperature errors, three hypothetical distributions are proposed (i.e., fit distribution in Table 4). The normal distribution is mentioned in the derivation in Section 4.2.3. The half-normal distribution is a fold of a normal distribution at its mean. For the residential building medium uncertainty level, a half-normal distribution was adopted. This can be attributed to the fact that almost no temperature decrease action was observed and thus the errors were all above zero. Constants were used for the residential building and the bakery under the low uncertainty level because the frequency of the setpoint-changing is too low (nearly zero) to follow any distributions.

Chi-square goodness of fit tests [44] at a rejection level of 1% were conducted to evaluate whether the proposed hypothetical distributions fit well. The types of fitting distributions, p-values of the tests, and the distribution parameters are reported in Table 4. In the table, μ is the mean and σ is the standard deviation of the normal/half-normal distribution. The null hypothesis here is that the room temperature prediction error follows the hypothetical distribution. The p-value is the evidence against this null hypothesis. Since all p-values are greater than 99%, all error distributions failed to reject the hypothesis at the level of 1%. This means they all follow the corresponding hypothetical distribution.

Table 4 Chi-square goodness of fit test p-values and normal distribution parameters.

Building	Uncertainty	Fit Distribution	p-value	μ [°C]	σ [°C]
Residential	Low	Constant	1.0	-6.45E-05	N/A
	Medium	Half-normal	0.999	-3.57E-01	4.35E-01
	High	Normal	0.999	1.56E+00	8.17E-01
Ice Cream Shop	Low	Normal	0.999	-3.48E-03	7.86E-03
	Medium	Normal	0.999	-4.45E-03	8.59E-03
	High	Normal	0.999	1.60E-02	1.59E-02
Bakery	Low	Constant	1.0	-3.42E-03	N/A
	Medium	Normal	0.999	3.01E-02	1.05E-01
	High	Normal	0.999	5.33E-01	4.65E-01

The frequency histogram and probability density functions (PDFs) of each building under various uncertainty levels are plotted in Figure 6. In the figure, it can be seen that the higher the uncertainty, the wider the room temperature range. This is because in scenarios with a higher uncertainty, occupants change the thermostat more frequently, which expands the possible temperature ranges. We also noticed that the temperature range in the ice cream shop is relatively concentrated compared to the other two buildings. This can be attributed to the large thermal mass of the building.

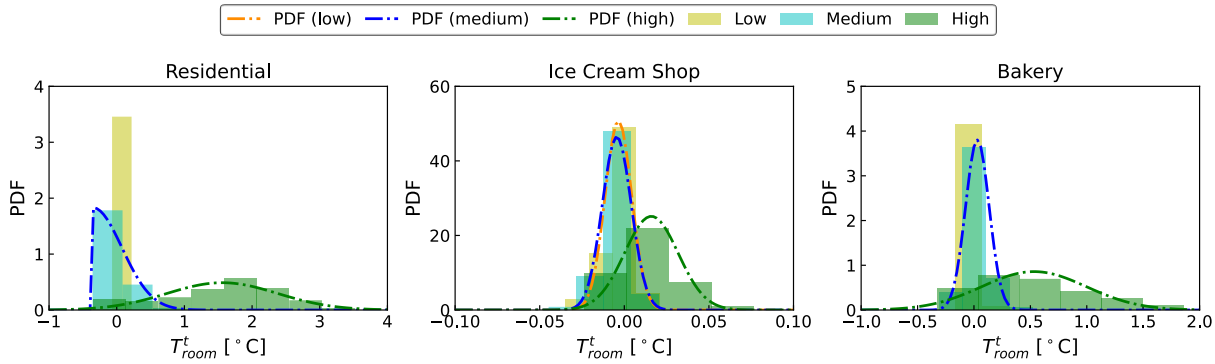

Figure 6 Room temperature prediction error PDFs obtained from the Monte Carlo simulations.

For the scenario where the temperature prediction error follows the half-normal distribution, we applied the chance constraint only to the upper bound because only increasing actions happen in this scenario. For the two scenarios where the room temperature error is estimated to be a constant, we adopted the original temperature bounds of [20ºC, 25ºC] because the estimated errors in both scenarios are smaller than 0.01ºC. We choose the $\epsilon_T = 1\%$ to ensure a 99% probability of abidance of the temperature constraints (Equation (24)). Table 5 lists the updated room temperature lower and upper bounds for each building under different scenarios.

Table 5 Room temperature bounds for chance-constrained optimizations.

Building	**Uncertainty**	$\underline{T}_{room}$ **[ºC]**	$\overline{T}_{room}$ **[ºC]**
Residential	Low	20.000	25.000
	Medium	20.000	24.236
	High	20.547	21.343
Ice Cream Shop	Low	20.024	24.983
	Medium	20.027	24.982
	High	20.025	24.943
Bakery	Low	20.000	25.000
	Medium	20.240	24.700
	High	20.664	23.273

5.3 Results and Discussions

This section first quantifies the impact of introducing occupant behavior uncertainties to the optimal scheduling problem. Then, the deterministic and chance-constrained controllers are tested on the community virtual testbed. Their control performance in terms of the unserved load ratio, the required battery size, and the unmet thermal preference hours are then compared.

5.3.1 Impact of Uncertainty

Figures 7 to 9 depict the occupant thermal preference and the corresponding room temperatures. In the figures, the upper plots show the simulated stochastic thermostat-changing actions at different uncertainty levels, where increase means a setpoint increase action, and vice versa. The lower plots show the resulting room temperatures with dashed lines.

The results of the low uncertainty scenario overlap with that of the baseline scenario (i.e., the deterministic scheduler without uncertainty) mainly due to the low probability of setpoint-changing actions in this scenario. With the increase in the probability, we see more frequent setpoint-changing actions in all three buildings. Further, the increase action happens more frequently than the decrease action. This is because between the temperature range of 20ºC and 24ºC, the probability of increase is much higher than that of decrease (see Figure 4). This also implies that the occupants' temperature preference is closer to 24ºC than 20ºC. Additionally, for the residential building and the bakery, the temperature difference between scenarios is more noticeable than for the ice cream shop; this is attributable to the different building thermal masses of the three buildings.

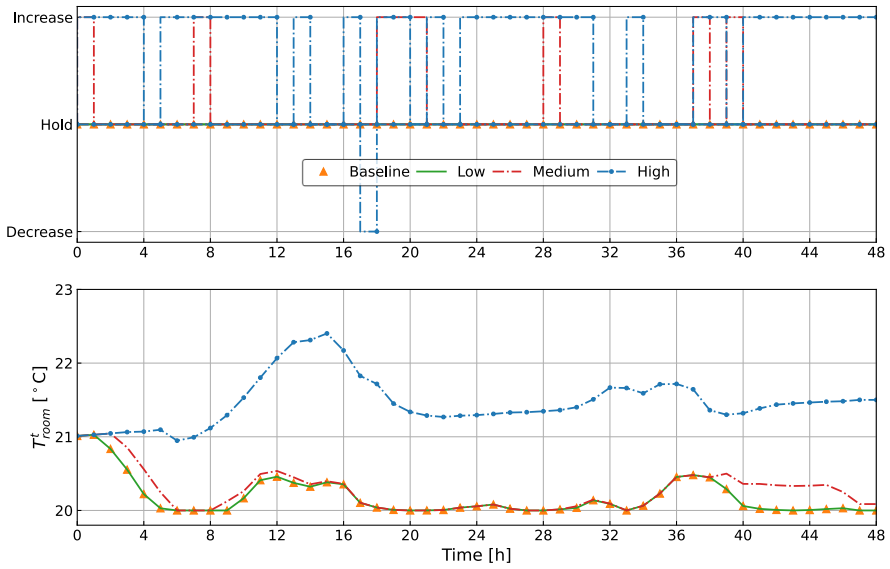

Figure 7 Residential building occupant thermostat changing actions (upper) and resulting room temperatures (lower) under three levels of uncertainty.

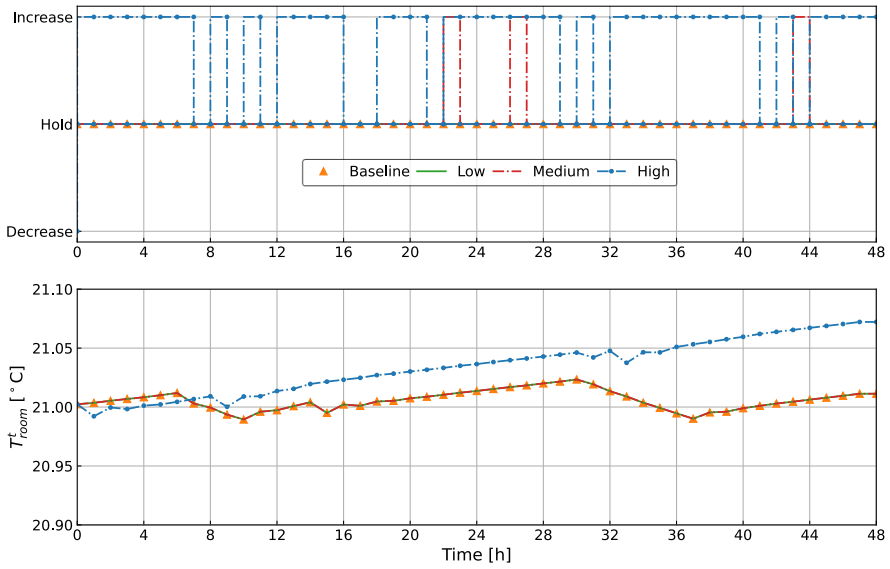

Figure 8 Ice cream shop occupant thermostat changing actions (upper) and resulting room temperatures (lower) under three levels of uncertainty.

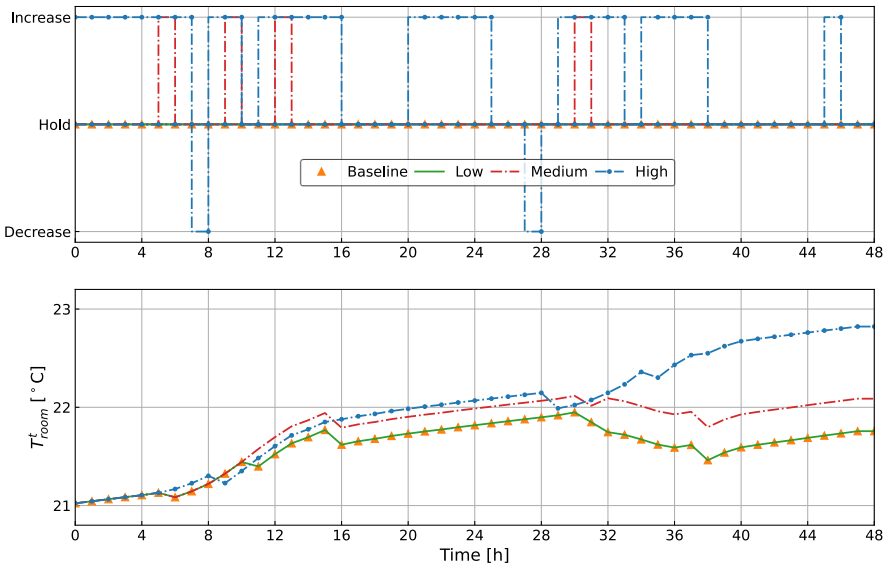

Figure 9 Bakery occupant thermostat changing actions (upper) and resulting room temperatures (lower) under three levels of uncertainty.

Table 6 lists the values of the KRIs in correspondence with Figures 7 to 9. The HVAC energy and average room temperature over the optimization horizon are also provided to facilitate the analysis of the results.

Table 6 Key resilience indicators for studied buildings under different uncertainty levels.

Building	Scenario	Unserved Load Ratio	Battery Size [kWh]	HVAC Energy [kWh]	Mean Room Temperature [°C]
Residential	Baseline	0.0744	47.686	32.139	20.185
	Low	0.0744	47.686	32.139	20.185
	Medium	0.0744	47.168	32.099	20.271
	High	0.0744	38.541	21.400	21.468
Ice Cream Shop	Baseline	0.0215	99.139	32.703	21.006
	Low	0.0215	99.139	32.703	21.006
	Medium	0.0215	99.139	32.703	21.006
	High	0.0215	93.166	10.063	21.033
Bakery	Baseline	0.0247	80.007	35.144	21.579
	Low	0.0247	80.007	35.144	21.579
	Medium	0.0247	73.496	27.604	21.766
	High	0.0247	76.801	11.310	21.973

From the table, we see that the unserved load ratio remains the same across all scenarios for each building. This can be attributed to the fact that in the controller design phase, the optimization objective is set to minimize the unserved load ratio. Hence, the unserved load ratios for each building are already minimal and are not affected by the occupants' thermostat-overriding behavior uncertainties. Instead, the battery-charging/discharging behavior is affected, as reflected by the different required battery sizes in the table. Note that the unserved load ratios are minimal, but not zero, because of our assumption that each shiftable load operates once and only once per day.

For the rest of the metrics, note that the battery size, HVAC energy, and the average room temperature remain the same for the baseline and low uncertainty scenarios in all buildings. This is because no setpoint-changing actions happened due to the relatively low probabilities, as shown in the figures above. As for the medium uncertainty scenarios, both the residential building and the bakery show higher room temperatures and lower HVAC energy while the ice cream shop still has the same results as the baseline, given its large thermal mass.

In terms of the high uncertainty scenarios, due to the prominent increase in room temperatures, we noticed more HVAC energy savings in all buildings. Note that though the average room temperature increase is insignificant, the HVAC energy savings is large due to the cumulative effect over the many hours of setpoint increase. Overall, we see a positive correlation between the HVAC energy and the required battery size. When the PV generation and the other building loads remain the same, the more HVAC energy, the larger required battery size. However, one opposite case was noted in the bakery high uncertainty scenario where the required battery size is slightly larger in the high uncertainty scenario than in the medium uncertainty scenario. This was caused by a setpoint decrease action at hour 28, which resulted in a battery discharging during the night and thus a smaller minimum SOC of the battery.

To summarize, occupant thermostat-changing behavior uncertainty needs to be considered when designing optimal schedulers for resilient buildings because it affects the indoor room temperature, the HVAC power, and thus the sizing of batteries. For the whole community, when considering the highest occupant behavior uncertainty, the consumed HVAC energy can be 57.2% less and the battery 8.08% smaller. Whereas the aforementioned impact depends on the uncertainty level (i.e., how frequently the occupants change the setpoint), heating or cooling season, and the occupants'

actual preference for the indoor room temperature compared to the room temperature designed by the scheduler. In our case, a preferred higher indoor room temperature saves HVAC energy. During the heating season, the observations could be the reversed.

5.3.2 Controller Performance

To further evaluate the performance of the chance-constrained controller in comparison with the deterministic controller, tests were run on the virtual testbed [28] in a stochastic manner. In each of the studied buildings, both the deterministic controller and the chance-constrained controller were tested for two days (i.e., August 4 and 5) with the three levels of uncertainties. The testing method is similar to the method proposed in Section 4.2.2. Additionally, the precalculated optimal battery charging/discharging, as well as the optimized loads, are also implemented in the testbed. One hundred repeated Monte Carlo simulations were run for each scenario to better observe the controller performance. The KRIs of the unserved load ratio, the required battery size, and the unmet thermal preference hours are adopted for the performance evaluation.

The upper plot of Figure 10 depicts the predetermined optimal schedules of the heat pump speed ratio as the inputs of the test. The lower plot then shows the corresponding room temperatures predicted by the linear regression models in the optimization. The data for the residential building is adopted here for the analysis. The plots for the ice cream shop and the bakery can be found in Appendix A. From the figure, we see that the scheduled speed ratios in the low and medium uncertainty scenarios overlap with that of the deterministic scheduler. Whereas the high uncertainty scenario tends to have lower speed ratios over the whole optimization horizon. This can be attributed to the controller settings shown in Table 5, where the temperature bounds set in the low and medium uncertainty scenarios are closer to the original bounds of [20ºC–25ºC]. Hence, the temperature constraints are not binding in these two scenarios. However, in the high uncertainty scenario, the temperature constraint is binding, which leads to the speed ratio reductions. As a result, a higher room temperature can be seen in the high uncertainty scenario.

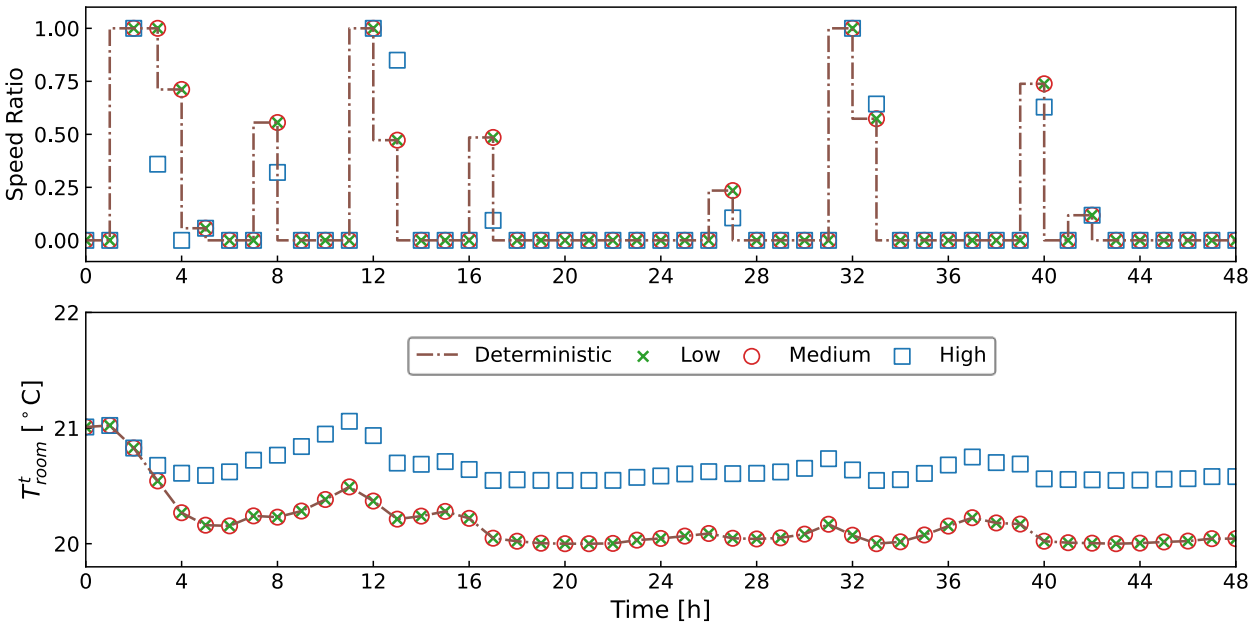

Figure 10 Optimal schedules of the heat pump speed ratio and predicted room temperatures by various schedulers (residential building).

Figures 11 to 13 depict the room temperature boxplots as the controller testing outputs. The lower and upper borders of the boxes represent the 25th and 75th percentiles of the data, respectively. The longer the box, the more scattered the room temperature. The lines inside the boxes represent the median values. The lines beyond the boxes represent the minimum and maximum values except for outliers, which are not shown in these figures. Note in the figures that the temperatures first concentrate together (shown as black lines) and then spread out (shown as boxes). This is because at the beginning of the simulations, no overriding behavior of the setpoints happens and the heat pump operates following the scheduled speed ratio. Once the overriding happens at a certain timestep in some simulations, the room temperature trends start to deviate and become boxes. The occupant-preferred temperature lines are also shown as orange lines in these figures as a reference; they are average setpoints adjusted by the occupants in all the Monte Carlo tests.

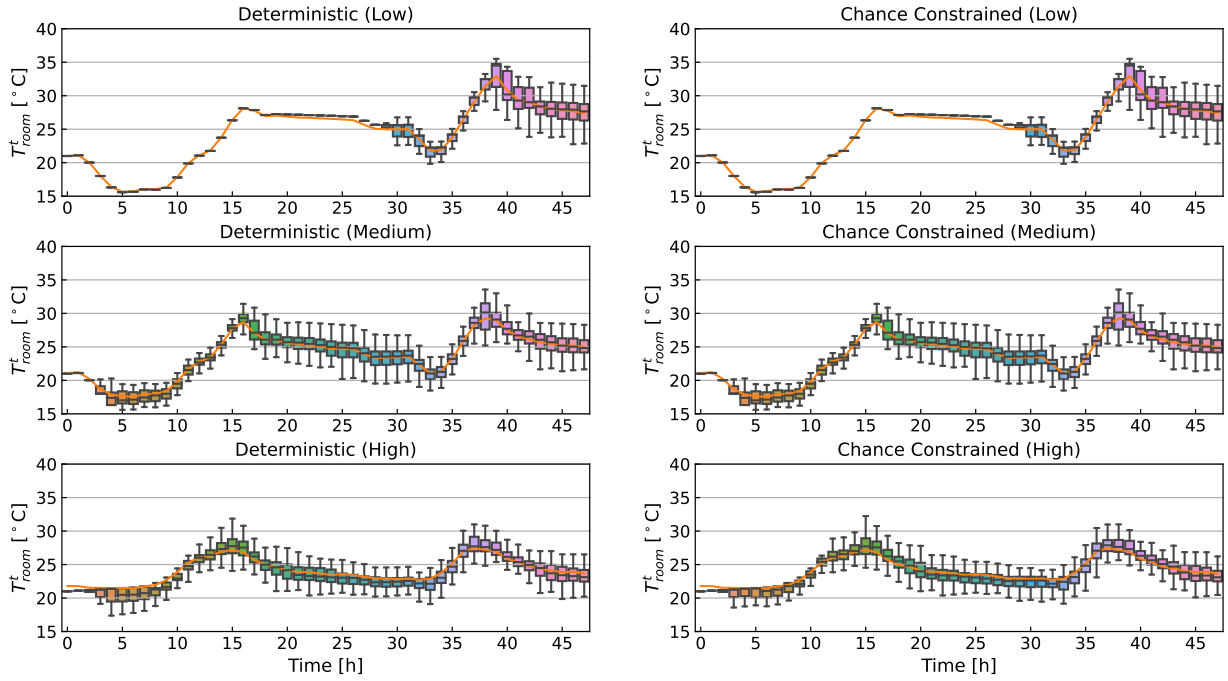

Figure 11 Residential building room temperature boxplots for control testing results.

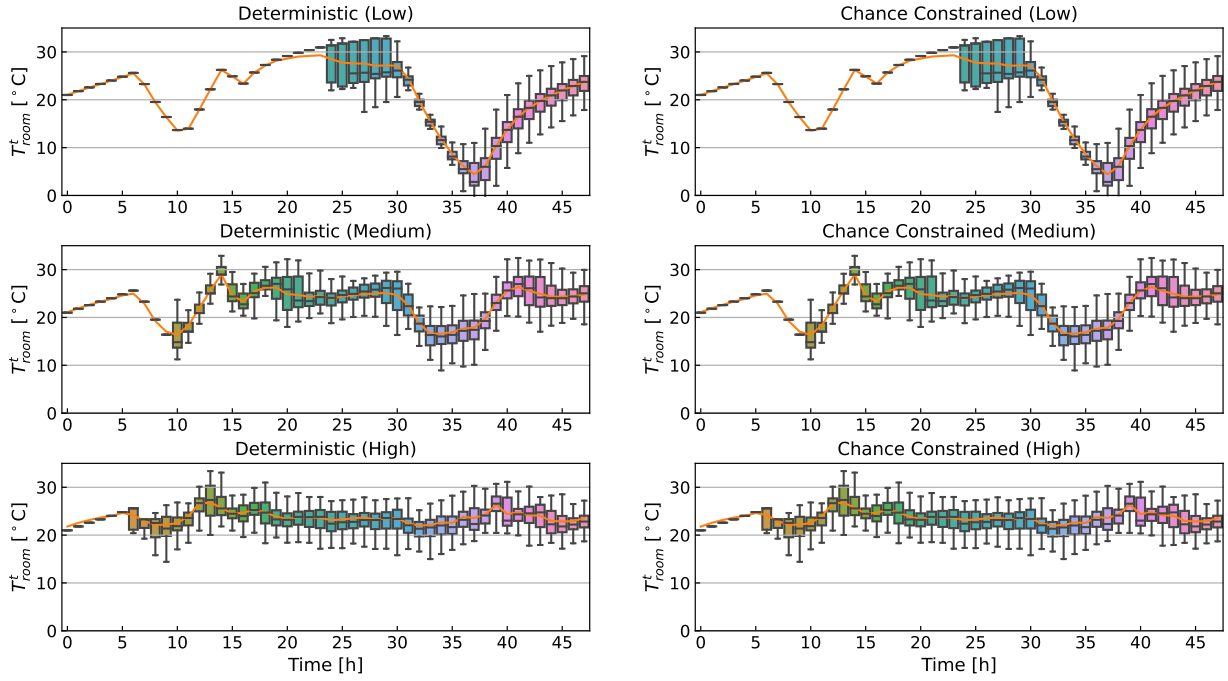

Figure 12 Ice cream shop room temperature boxplots for control testing results.

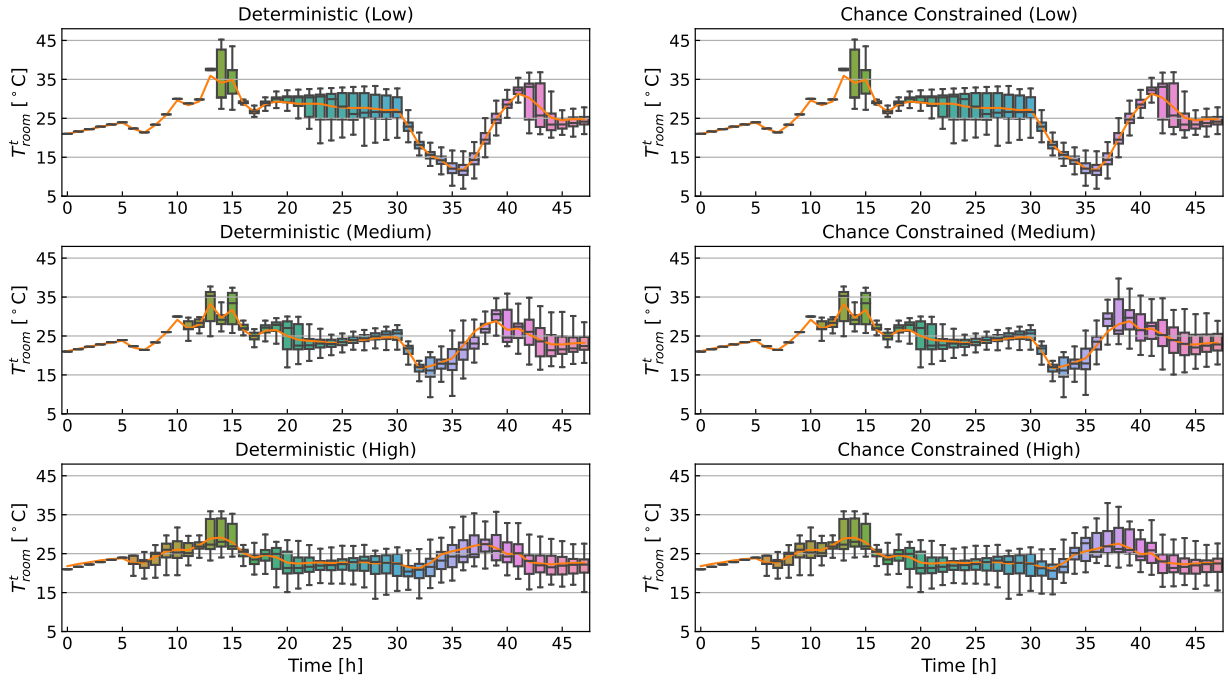

Figure 13 Bakery room temperature boxplots for control testing results.

In the figures, we see a general trend of narrower room temperature ranges from the low uncertainty scenarios to high uncertainty scenarios. This is due to the introduction of the occupant setpoint-overriding mechanism, which tends to moderate the extreme room temperatures. Also, there is a plant-model mismatch, which describes the parametric uncertainty of modeling that originates from neglected dynamics of the plant [25]. In our case, the mismatch exists as the simulated room temperatures in the testbed are slightly higher than those predicted by the reduced-order linear HVAC models. This is understandable because the physics-based testbed has a much higher fidelity and simulates the non-linearity of the real mechanical systems.

Because the difference in the room temperature between the two controllers is not depicted in these figures, Table 7 and Table 8 provide further quantitative evaluations of the room temperatures along with other controller performance. Additionally, note that the optimal schedules of some scenarios remain the same because of the unbinding temperature constraints, which led to the same testing outputs. Here we only discuss the scenarios that have different inputs and outputs. A full list of all testing results is available in Table A-2.

Table 7 Comparison of controller performance in the residential building high uncertainty scenario.

Controller	Unmet Thermal Preference Hours [ºC·h]	Mean Room Temperature [ºC]	Unserved Load Ratio	Required Battery Size [kWh]
Deterministic	48.91	23.75	0.074	47.69
Chance-constrained	46.42	23.87	0.074	44.12

In Table 7, we see a larger value of unmet thermal preference hours in the deterministic controller than the chance-constrained one. This can be attributed to the higher room temperatures regulated by the chance constraints to better satisfy the occupants' thermal preferences. Again, the same unserved load ratio is observed in both controllers because it is already minimal, which is enforced by the objective function. In terms of the battery size, the chance-constrained controller shows a smaller required battery size than the deterministic controller. This results from the fact that a higher room temperature has led to less consumed HVAC energy in the chance-constrained scenario. Thus, less discharging from the battery was happening, which led to a smaller required battery size. For the bakery results shown in Table 8, the same trends for the battery size and the unserved load ratio as the residential building can be observed under each uncertainty level. Namely, smaller batteries and the same unserved load ratios.

Table 8 Comparison of controller performances in the bakery medium and high uncertainty scenarios.

Uncertainty	Controller	Unmet Thermal Preference Hours [ºC·h]	Mean Room Temperature [ºC]	Unserved Load Ratio	Required Battery Size [kWh]
Medium	Deterministic	88.80	24.27	0.025	80.01
	Chance-constrained	91.28	24.50	0.025	76.89
High	Deterministic	102.81	23.65	0.025	80.01
	Chance-constrained	101.61	23.89	0.025	76.89

As for the unmet thermal preference hours, different trends are witnessed in the medium and high uncertainty levels. In the medium level, the deterministic controller shows fewer unmet preference hours than the chance-constrained controller. Whereas in the high uncertainty level, an opposite trend is seen. This is reasonable as we see a generally higher mean room temperature regulated by the chance-constrained controller under different uncertainty levels. However, in the medium scenario, a lower preference temperature line was obtained from the Monte Carlo testing, which is closer to the actual room temperatures of the deterministic controller. When the preference temperature rises in the high uncertainty scenario, the chance-constrained controller outperforms the deterministic controller with a higher actual room temperature and thus smaller unmet thermal preference hours.

When we compare different uncertainty levels in the bakery, we see that the mean room temperature decreases with the increase in uncertainty. This is because the lower temperature upper bounds shown in Table 5 have regulated the room temperature to sink when the uncertainty gets higher. Additionally, as seen in Figure 4, in the temperature range of 20ºC to 24ºC, the probability of increasing the temperature setpoint is much higher than that of decreasing it While above 24ºC, the probability to increase and to decrease is almost the same. This has caused the room temperatures to end up around 24ºC in the high uncertainty scenarios for all buildings (Table A-2). This reveals that with the increase in the occupant thermostat-changing uncertainties, the room temperatures tend to get closer to the occupants' preferred room temperature.

Though some improvement was noticed in the chance-constrained controller compared to the deterministic controller, the overall improvement was less than expected. This could be attributed to the following three factors. First, the impact of the uncertainty level on the controller performance improvement is prominent as we observe higher performance improvement in high uncertainty scenarios. Second, the thermal property, especially thermal mass, of the building itself also affects the results. Thermal mass serves as a thermal buffer to filter the impact of various HVAC supply temperatures. Hence, buildings with a larger thermal mass tend to experience less impact from the occupant thermal preference uncertainty. This can be demonstrated by the results of the ice cream shop, where the two controllers perform the same. Third, the plant-model mismatch also plays a significant role in the transition from the optimal scheduler design to its implementation. In the design phase, a series of control-oriented linear regression building models

was used. However, the testing took place on a high-fidelity physics-based testbed, where the complex system dynamics of the whole buildings and HVAC systems were modeled with shorter simulation timesteps. This is a common source of uncertainty to be addressed for MPC design and implementation.

In our opinion, joint effort from building scientists, modelers, and engineers is needed to facilitate implementing stochasticity in the building domain and ultimately better serve the occupants. For example, an open-source database focused on building performance related stochasticity such as the occupant behavior and weather forecast needs to be established. Further, readily available stochastic simulation tools need to be developed (e.g., Occupancy Simulator [45]). Finally, stochasticity needs to be incorporated into the whole process of building modeling and design in the form of boundary conditions or internal components.

6 Conclusion

In this paper, we proposed a preference-aware scheduler for resilient communities. Stochastic occupant thermostat-changing behavior models were introduced into a deterministic load scheduling framework as a source of uncertainty. The impact of occupant behavior uncertainty on community optimal scheduling strategies was discussed. KRIs such as the unserved load ratio, the required battery size, and the unmet thermal preference hours were adopted to quantify the impacts of uncertainties. Generally, the proposed controller performs better in terms of the unmet thermal preference hours and the battery sizes compared to the deterministic controller. Though only tested on three buildings of the studied community, the methodology of introducing occupant behavior uncertainty into load scheduling and testing can be generalized and applied to other building and behavior types.

More specifically, we determined that occupant thermostat-changing behavior uncertainty should be considered when designing optimal schedulers for resilient communities. For the whole community, when considering the highest occupant behavior uncertainty, the consumed HVAC energy can be 57.2% less and the battery 8.08% smaller. During the controller testing phase, the proposed chance-constrained controller proves its advantage over the deterministic controller by better serving the occupants' thermal needs and demonstrating a savings of 6.7 kWh of battery capacity for the whole community. Additionally, we noticed that with the presence of occupant

thermostat-changing uncertainties, the room temperatures tend to get closer to the occupants' preferred room temperature.

During the simulation experiments, we noticed some limitations of the proposed work. Because the proposed uncertainty method mainly deals with the uncertainty through the temperature constraints, it can be less effective for buildings of larger thermal mass due to the insensitivity to temperature constraints. Also, plant-model mismatch was noticed in the controller testing phase, which is a common parametric uncertainty that originates from neglected dynamics of the plant [25]. Finally, we used the thermostat changing models developed based on data from private office spaces in different building types, which can be debatable. Future work for this research includes extending the scope to heating scenarios to further generalize the findings. Additionally, real-time MPC control techniques could be integrated into the framework to overcome the lack of flexibility in *a priori* designed controllers.

Acknowledgements

This research is partially supported by the National Science Foundation under Awards No. IIS-1802017. It is also partially supported by the U.S. Department of Energy, Energy Efficiency and Renewable Energy, Building Technologies Office, under Contract No. DE-AC05-76RL01830. This work also emerged from the IBPSA Project 1, an internationally collaborative project conducted under the umbrella of the International Building Performance Simulation Association (IBPSA). Project 1 aims to develop and demonstrate a BIM/GIS and Modelica Framework for building and community energy system design and operation.

Appendix A

Table A-1 Complete list of building loads and heat gain coefficients [31–33].

Building	No.	Load	Capacity [W]	Heat Gain Coefficient	Heat Gain [W]	Weighted Average Coefficient
Residential	1	Lights	293	0.8	234.4	0.31
	2	Refrigerator	494	0.4	197.6	
	3	Computer	18	0.15	2.7	
	4	Range	1775	0.34	603.5	

Building	No.	Load	Capacity [W]	Heat Gain Coefficient	Heat Gain [W]	Weighted Average Coefficient
	5	Washer	438	0.8	350.4	
	6	Dryer	2795	0.15	419.25	
Ice Cream Shop	1	Lights	135	0.8	108	0.35
	2	Coolers	7394	0.4	2957.6	
	3	Display case	280	0.4	112	
	4	Coffee maker	2721	0.3	816.3	
	5	Soda dispenser	201	0.5	100.5	
	6	Outdoor ice storage	1127	0	0	
Bakery	1	Lights	1859	0.8	1487.2	0.38
	2	Coolers	4161	0.4	1664.4	
	3	Display case	1011	0.4	404.4	
	4	Range	4065	0.15	609.75	
	5	Mixer	521	0.31	161.51	
	6	Gas oven	761	0.2	152.2	
	7	Room plugs	377	0.5	188.5	
	8	Microwave	1664	0.67	1114.88	
	9	Dishwasher	1552	0.15	232.8	

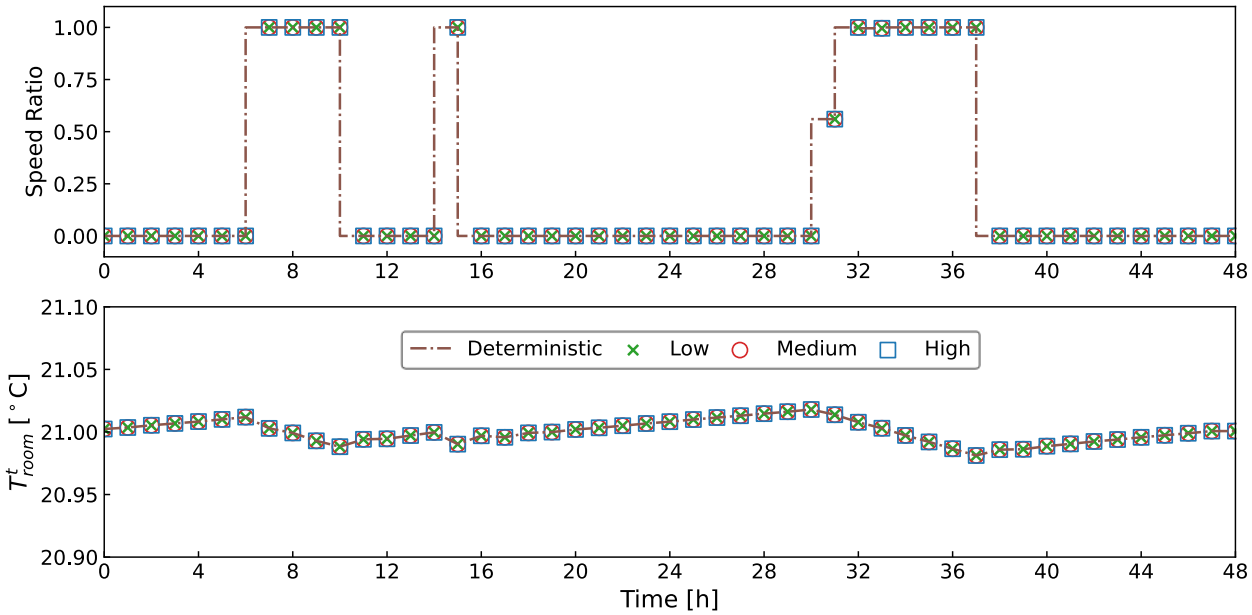

Figure A-1 Optimal schedules of the heat pump speed ratio and predicted room temperatures by various schedulers (ice cream shop).

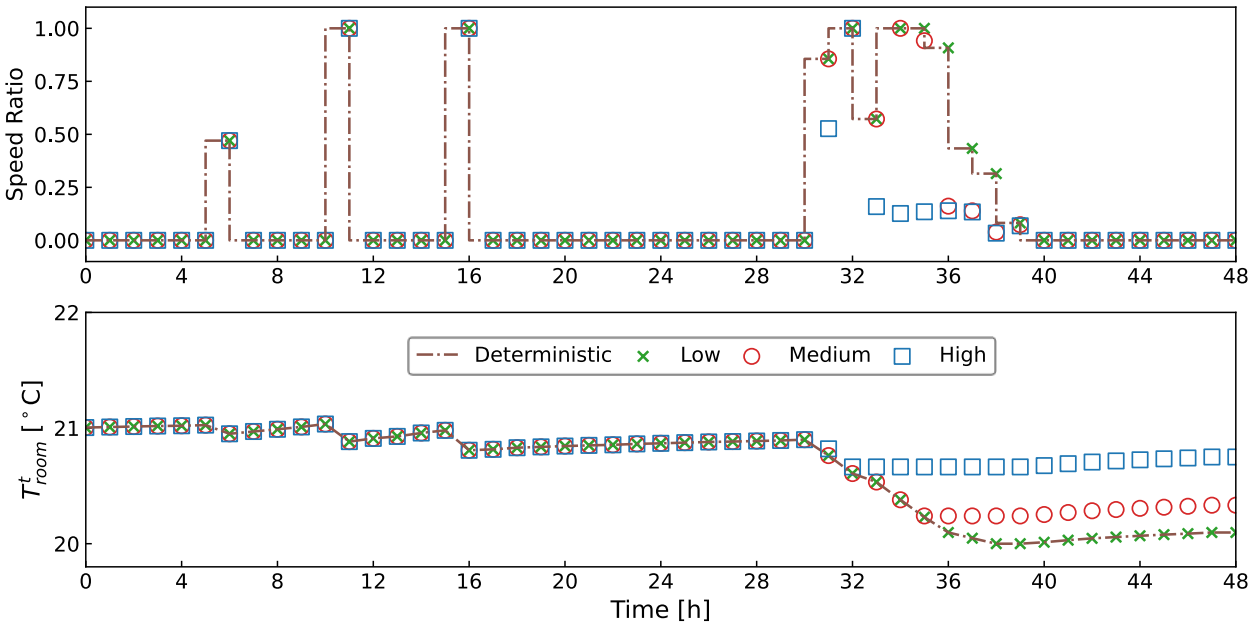

Figure A-2 Optimal schedules of the heat pump speed ratio and predicted room temperatures by various schedulers (bakery).

Table A-2 Full comparison of controller performances under different uncertainty levels in all three buildings.

KRIs	Controller	Residential			Ice Cream Shop			Bakery		
		Low	Medium	High	Low	Medium	High	Low	Medium	High
Unmet Thermal Preference Hours [°C·h]	Deterministic	33.70	47.19	48.91	70.69	85.61	86.87	89.03	88.80	102.81
	Chance-constrained	33.70	47.19	46.42	70.69	85.61	86.87	89.03	91.28	101.61
Mean Room Temperature [°C]	Deterministic	24.38	23.69	23.75	21.23	22.87	23.38	25.34	24.27	23.65
	Chance-constrained	24.38	23.69	23.87	21.23	22.87	23.38	25.34	24.50	23.89
Unserved Load Ratio	Deterministic	0.074			0.022			0.025		
	Chance-constrained	0.074	0.074	0.074	0.022	0.022	0.022	0.025	0.025	0.025
Required Battery Size [kWh]	Deterministic	47.69			99.14			80.01		
	Chance-constrained	47.69	47.69	44.12	99.14	99.14	99.14	80.01	76.89	76.89

References

[1] The Texas Tribune. Winter Storm 2021. https://www.texastribune.org/series/winter-storm-power-outage/ (accessed Apr 1, 2021).

[2] Wang, J.; Garifi, K.; Baker, K.; Zuo, W.; Zhang, Y. Optimal Operation for Resilient Communities through a Hierarchical Load Scheduling Framework. In *Proceedings of 2020 Building Performance Analysis Conference & SimBuild*; Virtual Conference, 2020.

[3] Wang, J.; Zuo, W.; Rhode-Barbarigos, L.; Lu, X.; Wang, J.; Lin, Y. Literature Review on Modeling and Simulation of Energy Infrastructures from a Resilience Perspective. *Reliab. Eng. Syst. Saf.*, **2019**, *183*, 360–373. https://doi.org/10.1016/j.ress.2018.11.029.

[4] Tang, H.; Wang, S.; Li, H. Flexibility Categorization, Sources, Capabilities and Technologies for Energy-Flexible and Grid-Responsive Buildings: State-of-The-Art and Future Perspective. *Energy*, **2020**, 119598. https://doi.org/10.1016/j.energy.2020.119598.

[5] Kou, X.; Li, F.; Dong, J.; Olama, M.; Starke, M.; Chen, Y.; Zandi, H. A Comprehensive Scheduling Framework Using SP-ADMM for Residential Demand Response with Weather and Consumer Uncertainties. *IEEE Trans. Power Syst.*, **2020**. https://doi.org/10.1109/TPWRS.2020.3029272.

[6] Faraji, J.; Ketabi, A.; Hashemi-Dezaki, H.; Shafie-Khah, M.; Catalão, J. P. S. Optimal Day-Ahead Self-Scheduling and Operation of Prosumer Microgrids Using Hybrid Machine Learning-Based Weather and Load Forecasting. *IEEE Access*, **2020**, *8*, 157284–157305. https://doi.org/10.1109/ACCESS.2020.3019562.

[7] Wang, J.; Garifi, K.; Baker, K.; Zuo, W.; Zhang, Y.; Huang, S.; Vrabie, D. Optimal Renewable Resource Allocation and Load Scheduling of Resilient Communities. *Energies*. 2020. https://doi.org/10.3390/en13215683.

[8] Yu, M. G.; Pavlak, G. S. Assessing the Performance of Uncertainty-Aware Transactive Controls for Building Thermal Energy Storage Systems. *Appl. Energy*, **2021**, *282*, 116103.

https://doi.org/10.1016/j.apenergy.2020.116103.

[9] Liang, Z.; Huang, C.; Su, W.; Duan, N.; Donde, V.; Wang, B.; Zhao, X. Safe Reinforcement Learning-Based Resilient Proactive Scheduling for a Commercial Building Considering Correlated Demand Response. *IEEE Open Access J. Power Energy*, **2021**, *8*, 85–96. https://doi.org/10.1109/oajpe.2021.3064319.

[10] Ahmad, A.; Khan, J. Y. Real-Time Load Scheduling, Energy Storage Control and Comfort Management for Grid-Connected Solar Integrated Smart Buildings. *Appl. Energy*, **2020**, *259*, 114208. https://doi.org/10.1016/j.apenergy.2019.114208.

[11] E Silva, D. P.; Salles, J. L. F.; Fardin, J. F.; Pereira, M. M. R. Management of an Island and Grid-Connected Microgrid Using Hybrid Economic Model Predictive Control with Weather Data. *Appl. Energy*, **2020**, *278*, 115581. https://doi.org/10.1016/j.apenergy.2020.115581.

[12] Yundra, E.; Surabaya, U. N.; Kartini, U.; Wardani, L.; Ardianto, D.; Surabaya, U. N.; Surabaya, U. N.; Surabaya, U. N. Hybrid Model Combined Fuzzy Multi-Objective Decision Making with Feed Forward Neural Network (F-MODMFFNN) For Very Short-Term Load Forecasting Based on Weather Data. *Int. J. Intell. Eng. Syst.*, **2020**, *13* (4), 182–195. https://doi.org/10.22266/IJIES2020.0831.16.

[13] Garifi, K.; Baker, K.; Christensen, D.; Touri, B. Stochastic Home Energy Management Systems with Varying Controllable Resources. In *2019 IEEE Power & Energy Society General Meeting (PESGM)*; IEEE: Atlanta, GA, USA, 2019; pp 1–5.

[14] Lu, M.; Abedinia, O.; Bagheri, M.; Ghadimi, N.; Shafie-khah, M.; Catalão, J. P. S. Smart Load Scheduling Strategy Utilising Optimal Charging of Electric Vehicles in Power Grids Based on an Optimisation Algorithm. *IET Smart Grid*, **2020**, *3* (6), 914–923. https://doi.org/10.1049/iet-stg.2019.0334.

[15] Khalid, Z.; Abbas, G.; Awais, M.; Alquthami, T.; Rasheed, M. B. A Novel Load Scheduling Mechanism Using Artificial Neural Network Based Customer Profiles in Smart Grid.

Energies, **2020**, *13* (5), 1062. https://doi.org/10.3390/en13051062.

[16] Kerboua, A.; Boukli-Hacene, F.; Mourad, K. A. Particle Swarm Optimization for Micro-Grid Power Management and Load Scheduling. *Int. J. Energy Econ. Policy*, **2020**, *10* (2), 71. https://doi.org/10.32479/ijeep.8568.

[17] Kaur, R.; Schaye, C.; Thompson, K.; Yee, D. C.; Zilz, R.; Sreenivas, R. S.; Sowers, R. B. Machine Learning and Price-Based Load Scheduling for an Optimal IoT Control in the Smart and Frugal Home. *Energy AI*, **2021**, *3*, 100042. https://doi.org/10.1016/j.egyai.2020.100042.

[18] Chung, H.-M.; Maharjan, S.; Zhang, Y.; Eliassen, F. Distributed Deep Reinforcement Learning for Intelligent Load Scheduling in Residential Smart Grids. *IEEE Trans. Ind. Informatics*, **2020**, *17* (4), 2752–2763. https://doi.org/10.1109/TII.2020.3007167.

[19] Aftab, M.; Chen, C.; Chau, C.-K.; Rahwan, T. Automatic HVAC Control with Real-Time Occupancy Recognition and Simulation-Guided Model Predictive Control in Low-Cost Embedded System. *Energy Build.*, **2017**, *154*, 141–156. https://doi.org/10.1016/j.enbuild.2017.07.077.

[20] Lim, B.; Van Den Briel, M.; Thiébaux, S.; Backhaus, S.; Bent, R. HVAC-Aware Occupancy Scheduling. In *Proceedings of the AAAI Conference on Artificial Intelligence*; 2015; Vol. 29.

[21] Jin, Y.; Yan, D.; Zhang, X.; An, J.; Han, M. A Data-Driven Model Predictive Control for Lighting System Based on Historical Occupancy in an Office Building: Methodology Development. In *Building Simulation*; Springer, 2020; pp 1–17. https://doi.org/10.1007/s12273-020-0638-x.

[22] Wang, J.; Zuo, W.; Huang, S.; Vrabie, D. Data-Driven Prediction of Occupant Presence and Lighting Power: A Case Study for Small Commercial Buildings. In *American Modelica Conference*; 2020.

[23] Chen, X.; Wang, Q.; Srebric, J. Model Predictive Control for Indoor Thermal Comfort and Energy Optimization Using Occupant Feedback. *Energy Build.*, **2015**, *102*, 357–369. https://doi.org/10.1016/j.enbuild.2015.06.002.

[24] West, S. R.; Ward, J. K.; Wall, J. Trial Results from a Model Predictive Control and Optimisation System for Commercial Building HVAC. *Energy Build.*, **2014**, *72*, 271–279. https://doi.org/10.1016/j.enbuild.2013.12.037.

[25] Drgoňa, J.; Arroyo, J.; Figueroa, I. C.; Blum, D.; Arendt, K.; Kim, D.; Ollé, E. P.; Oravec, J.; Wetter, M.; Vrabie, D. L. All You Need to Know about Model Predictive Control for Buildings. *Annu. Rev. Control*, **2020**. https://doi.org/10.1016/j.arcontrol.2020.09.001.

[26] Garifi, K.; Baker, K.; Touri, B.; Christensen, D. Stochastic Model Predictive Control for Demand Response in a Home Energy Management System. In *2018 IEEE Power & Energy Society General Meeting (PESGM)*; Portland, OR, USA, 2018; pp 1–5.

[27] Zhang, X.; Schildbach, G.; Sturzenegger, D.; Morari, M. Scenario-Based MPC for Energy-Efficient Building Climate Control under Weather and Occupancy Uncertainty. In *2013 European Control Conference (ECC)*; IEEE, 2013; pp 1029–1034.

[28] He, D.; Huang, S.; Zuo, W.; Kaiser, R. Towards to the Development of Virtual Testbed for Net Zero Energy Communities. In *SimBuild 2016: Building Performance Modeling Conference*; Salt Lake City, UT, USA, 2016; Vol. 6.

[29] Zakula, T.; Armstrong, P. R.; Norford, L. Modeling Environment for Model Predictive Control of Buildings. *Energy Build.*, **2014**, *85*, 549–559. https://doi.org/10.1016/j.enbuild.2014.09.039.

[30] The Engineering ToolBox. Metabolic Heat Gain from Persons. https://www.engineeringtoolbox.com/metabolic-heat-persons-d_706.html (accessed Feb 19, 2021).

[31] Hosni, M. H.; Beck, B. T. Updated Experimental Results for Heat Gain from Office

827 Equipment in Buildings. *ASHRAE Trans.*, **2011**, *117* (2).

828 [32] ASHRAE. *ASHRAE Handbook — Fundamentals 2017*; 2017.

829 [33] Lawrence Berkeley National Laboratory. Home Energy Saver & Score: Engineering
830 Documentation - Internal Gains. http://hes-documentation.lbl.gov/calculation-
831 methodology/calculation-of-energy-consumption/heating-and-cooling-
832 calculation/internal-gains (accessed Feb 16, 2021).

833 [34] Maslow, A. H. *Motivation and Personality*; Harper & Brothers: New York City, USA, 1954.

834 [35] Roth, A.; Reyna, J.; Christensen, J.; Vrabie, D.; Adetola, V. GEB Technical Report Webinar
835 Series: Whole-Building Control, Sensing, Modeling & Analytics
836 https://www.energy.gov/sites/default/files/2020/05/f74/bto-geb-webinar-CSMA-
837 051920.pdf.

838 [36] Zhao, Z.; Lee, W. C.; Shin, Y.; Song, K.-B. An Optimal Power Scheduling Method for
839 Demand Response in Home Energy Management System. *IEEE Trans. Smart Grid*, **2013**,
840 *4* (3), 1391–1400. https://doi.org/10.1109/TSG.2013.2251018.

841 [37] SiteSage. Historic Green Village Submetering Data.
842 https://sitesage.net/home/management/index.php (accessed Oct 7, 2020).

843 [38] Garifi, K.; Baker, K.; Christensen, D.; Touri, B. Control of home energy management
844 systems with energy storage: Nonsimultaneous charging and discharging guarantees
845 https://arxiv.org/pdf/1805.00100.pdf.

846 [39] Gunay, H. B.; O'Brien, W.; Beausoleil-Morrison, I.; Bursill, J. Development and
847 Implementation of a Thermostat Learning Algorithm. *Sci. Technol. Built Environ.*, **2018**,
848 *24* (1), 43–56. https://doi.org/10.1080/23744731.2017.1328956.

849 [40] Heirung, T. A. N.; Paulson, J. A.; O'Leary, J.; Mesbah, A. Stochastic Model Predictive
850 Control—How Does It Work? *Comput. Chem. Eng.*, **2018**, *114*, 158–170.
851 https://doi.org/10.1016/j.compchemeng.2017.10.026.

[41] The Modelica Association. Modelica. 2019.

[42] Huang, S.; Wang, J.; Fu, Y.; Zuo, W.; Hinkelman, K.; Kaiser, M. R.; He, D.; Vrabie, D. *An Open-Source Virtual Testbed for a Real Net-Zero Energy Community*; 2021.

[43] Mooney, C. Z. *Monte Carlo Simulation*; Sage, 1997.

[44] Statistics Solutions. Chi-Square Goodness of Fit Test. https://www.statisticssolutions.com/chi-square-goodness-of-fit-test/ (accessed Feb 25, 2021).

[45] Chen, Y.; Hong, T.; Luo, X. An Agent-Based Stochastic Occupancy Simulator. In *Building Simulation*; Springer, 2018; Vol. 11, pp 37–49.